Cr impurity-induced electronic states in ZnTe(110) surface

2015 Jpn. J. Appl. Phys. 54 08LB01

(http://iopscience.iop.org/1347-4065/54/8S2/08LB01)

Japanese Journal of Applied Physics **54**, 08LB01 (2015) **REGULAR PAPER**
http://dx.doi.org/**10.7567/JJAP.54.08LB01**

Cr impurity-induced electronic states in ZnTe(110) surface

Ken Kanazawa*, Taku Nishimura, Shoji Yoshida, Hidemi Shigekawa, and Shinji Kuroda

Faculty of Pure and Applied Sciences, University of Tsukuba, Tsukuba, Ibaraki 305-8573, Japan
E-mail: kanazawa@ims.tsukuba.ac.jp

Received November 12, 2014; accepted December 25, 2014; published online June 4, 2015

The impurity states of Cr atoms, which substituted Zn sites in the topmost layer of a p-type ZnTe(110) surface, were investigated by scanning tunneling microscopy/spectroscopy (STM/STS) and we firstly observed Cr-induced impurity states in the energy gap region of the host ZnTe including the unoccupied states by STS. Furthermore, we compared the observed energy levels and spatial distributions of the local density of states with those in the previous theoretical study [Katayama-Yoshida et al., Phys. Status Solidi A **204**, 15 (2007)] and successfully identified the impurity states as the respective spin-polarized impurity states predicted by the theoretical study.

1. Introduction

The investigation of electronic states of the magnetic impurities in a host semiconductor is essential in understanding the mechanism of ferromagnetism of diluted magnetic semiconductors (DMSs) and applying and controlling the states in future spintronic devices.[1,2] The magnetic interaction between transition-metal (TM) impurities in a magnetic semiconductor depends on the combination of the host semiconductor and the magnetic impurity elements. In order to realize a DMS material with high performance characteristics such as room-temperature (RT) ferromagnetism, we must understand the impurity states as well as possible systematically. Furthermore, from the viewpoint of technological applications, to advance the new research field of nanotechnology combined with magnetism, it is also important to investigate the magnetic behavior of the material down-sized to the atomic scale.

Scanning tunneling microscopy/spectroscopy (STM/STS) is one of the most powerful methods of studying such impurity states at a single-atom scale. Up to now, several STM studies for DMS systems mainly based on TM-doped GaAs have been reported.[3–15] According to those reports, distinct impurity states are induced by the hybridization of the impurity d levels of TM with the host. In particular, recently, for Fe atoms substituting into the Ga site on the GaAs(110) surface, Mühlenberend et al. observed impurity states located near the valence band maximum of the host GaAs, in good agreement with the prediction in an earlier theoretical study.[15]

Cr-doped ZnTe [(Zn,Cr)Te] has been regarded as one of the promising materials for spintronic devices because of its intrinsic RT ferromagnetism when the Cr composition is about 20%.[16] In order to clarify the origin of magnetic phenomena induced by the doped Cr atoms, it is essential to investigate the impurity states such as their energy levels and electronic spatial distributions. Several theoretical energy diagrams of the Cr impurity states in the band structure of the host ZnTe have been proposed.[17] However, the number of experimental reports is very few.[16,18,19] In one of our earlier experimental studies, we performed cross-sectional STM/STS measurements for (Zn,Cr)Te grown by molecular beam epitaxy and revealed that a Cr atom formed a localized state within the bandgap of the host ZnTe; this state was broadened for a pair of Cr atoms within a distance of ~1 nm owing to ferromagnetic interaction.[19] However, in that study, the impurity states only in the negative sample bias region were investigated; it is important to examine all the impurity states including the empty states in order to understand and apply them. Moreover, considering their application to future nanotechnology, it is meaningful to study the single TM atom that is adsorbed and substitutes into the cation site on the topmost surface of the host semiconductor without any influence of neighboring TM impurities. Here, we present the results obtained in a STM/STS study on Cr atoms adsorbed on a ZnTe(110) surface. In this study, we successfully observed Cr atoms substituting for Zn atoms in the topmost surface, and for the first time, report that their impurity states above the Fermi energy are in good agreement with the results of an earlier theoretical study. Furthermore, the results of our STS measurements suggest the possibility of splitting of the degenerate impurity states owing to the symmetry breaking at the surface.

2. Experimental methods

As the substrate, we prepared a ZnTe(110) clean surface by cleaving a single crystal p-type ZnTe(100) wafer (P-doped, $\sim 1 \times 10^{18}\,\mathrm{cm}^{-3}$) in a high vacuum ($\sim 10^{-5}\,\mathrm{Pa}$). We deposited Cr atoms on the surface at room temperature by the electron beam deposition method. The area covered by Cr atoms was very small in order to observe the electronic states of single Cr atoms. All STM and STS measurements were performed in an ultrahigh vacuum ($\sim 1 \times 10^{-9}\,\mathrm{Pa}$) at a liquid nitrogen temperature (~80 K) using an electrochemically sharpened W tip ($\phi = 0.3\,\mathrm{mm}$). STM images were obtained in the constant-current mode only at negative sample bias voltages, since the STM observation of the ZnTe(110) surface with a positive sample bias voltage is unstable, as reported by Wierts et al.[20] However, we could investigate the electronic states of the unoccupied states by STS using a setpoint at negative sample bias voltages. Differential conductance (dI/dV)–V curves were measured using a lock-in amplifier (3 kHz, $\Delta V_{\mathrm{p-p}} = 20\,\mathrm{mV}$) with open feedback loop conditions.

3. Results and discussion

Figure 1(a) shows a typical STM image of the ZnTe(110) surface obtained by the cleaving process. As shown in this image, the surface was quite flat and the numbers of defects and absorbates were very small. Since occupied lone pair states are formed on the topmost Te atoms owing to charge transfer from topmost Zn atoms, the Te atoms can be imaged as bright points at a negative sample bias voltage. In addition

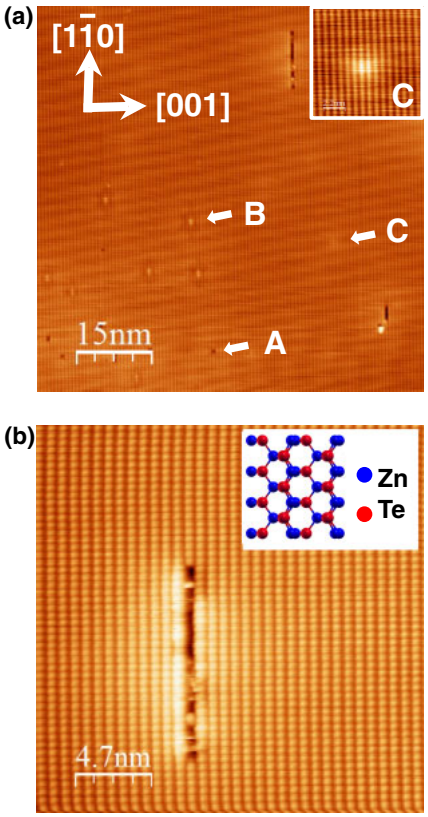

Fig. 1. (Color online) (a) STM image of ZnTe(110) surface ($V_s = -3.0$ V, $I_t = 20$ pA) before Cr adsorption. A, B, and C indicate three kinds of point defects found on the surface. The inset of (a) shows a magnified STM image of the point defect C. (b) High-resolution image of ZnTe(110) surface ($V_s = -2.0$ V, $I_t = 20$ pA). The inset of (b) shows a schematic structure of the ZnTe(110) surface.

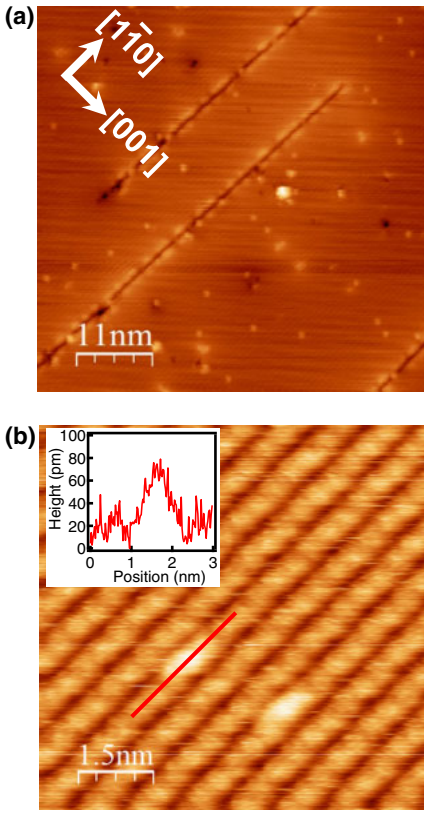

Fig. 2. (Color online) (a) STM image of Cr-adsorbed ZnTe(110) surface ($V_s = -2.5$ V, $I_t = 20$ pA). (b) STM image of single Cr atoms substituting into Zn sites in the first (110) atomic layer ($V_s = -2.5$ V, $I_t = 20$ pA). The inset shows the line profile measured along the red line in the STM image.

to the bright lines of Te atoms along the ⟨110⟩ direction, several dark lines along the same direction were also observed. According to the previous studies,[20,21] these dark lines are line defects caused by the absence of topmost atoms and are intrinsic defects of the ZnTe(110) surface. From the different brightnesses on the two sides of the dark-line defects, which are intrinsic defects of the ZnTe(110) surface, we can determine the indexes of the unit vectors on the surface ([001] and [1$\bar{1}$0] directions), as shown in Fig. 1(a).[21] We could also determine the correspondence of the STM image to the atomic arrangement on the surface, as shown in Fig. 1(b). Even in the clean surface, several point defects were observed, as indicated by A, B, and C. Since the defect labeled A is a depression in the single-atom scale, we identified it as a single-atom deficiency of surface atoms. The defect labeled B is imaged as a single-atom protrusion, with a height of about 1 Å. From this result, it is likely to be an adsorbed atom on the surface. These two kinds of defects should be generated by the cleavage. On the other hand, the defect labeled C, which is observed as a protrusion with spatial broadening larger than 3 nm diameter in the surface, corresponds to a phosphorus atom doped as an acceptor, since the appearance is very similar to that of an acceptor nitrogen atom in ZnTe, as reported in an earlier STM study by Wierts et al.[20]

After the adsorption of Cr atoms, a large number of small protrusions with bright contrast corresponding to Cr atoms were observed [Fig. 2(a)]. A typical STM image of adsorbed Cr atoms at $V_s = -2.5$ V is shown in Fig. 2(b). Most of them were imaged as bright points on the topmost Te atomic row with similar size and brightness to those of the Cr atoms observed in our previous cross-sectional STM study for MBE-grown (Zn,Cr)Te.[19] After comparison with the results of the previous study, we concluded that the bright points, whose STM topographic heights are ∼0.35 Å larger than that of topmost Te atoms [inset of Fig. 2(b)], correspond to Cr atoms substituting for Zn atoms in the first layer of the surface. According to the theoretical study performed in our previous study,[19] when a Cr atom substitutes a Zn atom in the topmost (110) surface layer, the region around the topmost two Te atoms neighboring with the Cr is bright in the STM image at a negative sample bias voltage, reflecting the impurity state induced by the Cr atom. Such substitutions of adsorbed TM atoms for cation sites in semiconductor surfaces without any STM manipulation have been observed in several studies.[13,15]

Next, in order to investigate the impurity states in more detail, we carried out STS measurements above a substitutional Cr atom at the points shown in Figs. 3(a) and 3(b). Since the ZnTe(110) surface is unstable for STM observation at a positive sample bias voltage, as described above, we realized STS measurement of the full spectrum by using a set point at a negative sample bias voltage. Figure 3(c) shows the dI/dV–V spectra, which correspond to the energy dependence of the local density of states (LDOS), obtained at the positions shown in (a) and over the surface without Cr atoms. The colors of the spectra correspond to those of the closed circles marking the measurement points in (a). Figure 3(d)

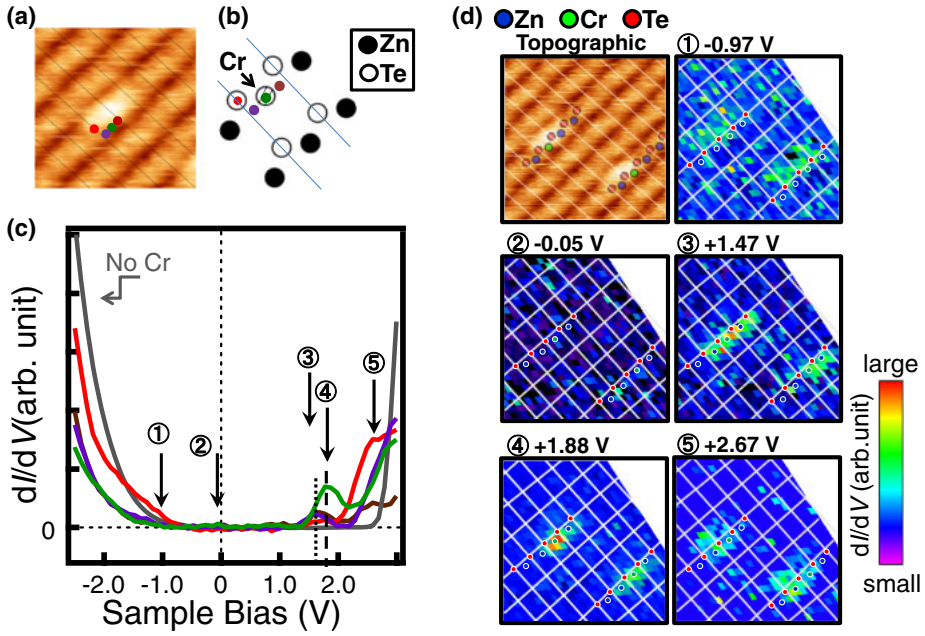

Fig. 3. (Color online) (a) STM image of the Cr atom on which STS measurements were carried out ($V_s = -2.5$ V, $I_t = 20$ pA). (b) Schematic of the atomic structure shown in (a), with the positions where STS measurements were carried out. (c) dI/dV–V spectra obtained at the positions shown in (a). The colors of the spectra correspond to those of the closed circles marking the measurement points in (a). (d) dI/dV maps over the two substitutional Cr atoms to show the spatial distribution of the energy states shown in (c). White lines correspond to the atomic rows of Te along the [1$\bar{1}$0] and [001] directions in the topmost surface. These lines are developed from the topographic STM image of this region (top left). Te atoms in the topmost surface should be located at the intersections of the two lines. The positions of Cr atoms are indicated using a superposed atomic structural model and indicated by colored circles surrounded by a white line in the images.

shows the dI/dV maps obtained over the two substitutional Cr atoms to show the spatial distribution of the energy states shown in (c). Bias voltages slightly different from those at the peak positions shown in (c) were used to enhance the image of each energy state by reducing the overlap of their spectra. The positions of atomic rows of topmost Te atoms along the [1$\bar{1}$0] and [001] directions are shown by white lines in Fig. 3(d). As an example of a map at a sample bias voltage without any specific electronic states in the dI/dV–V spectra, dI/dV values in Fig. 3(d#2), which was obtained at $V_s = -0.05$ V, were almost zero uniformly all over the observed area.

The spectrum obtained over the area without Cr is almost zero in the bias voltage range $-0.7 < V_s < 2.2$ V, reflecting the electronic states of a p-type semiconductor with the effect of tip-induced band bending (TIBB), which becomes larger at a negative sample bias for a p-type semiconductor. The dI/dV spectra measured around the Cr atoms clearly exhibited a larger dI/dV than that obtained over the area of ZnTe without Cr in the small bias region ($-1.0 < V_s < +2.5$ V). This result shows the existence of Cr impurity states within the bandgap of the ZnTe.

Here, in order to clarify the origin of the peaks, we compare the STS result with the results of the previous theoretical study reported by Katayama-Yoshida et al.[17] They calculated the DOS of the (Zn,Cr)Te crystal, in which Cr atoms substitute into the tetrahedral Zn site. The theoretical study has revealed the existence of spin-polarized impurity states formed by the hybridization between the 3d electrons of substitutional Cr atoms and the 5p electrons of Te atoms, which mainly contribute to the electronic states of the valence band of the host ZnTe, namely, the bonding state (t^b), antibonding state (t^a), and nonbonding state (e). We present a simple schematic overview of the energy diagram of the electronic structure of Cr^{2+} at the tetrahedral substitutonal site, as shown in Fig. 4(a), derived from the DOS calculated in the theoretical study.

Firstly, the dI/dV indicated by the red line in Fig. 3(c) was measured on the atomic row of the topmost Te atoms and was larger than that obtained over the area of ZnTe without Cr in the small negative bias voltage range $-0.65 < V_s < -1.5$ V, labeled #1 in Fig. 3(c). The LDOS [Fig. 3(d#1)] is large at the topmost atomic row of Te atoms near the Cr atoms. From the comparison of these results with the energy diagram and the results of our previous study,[19] it is concluded that the larger dI/dV labeled #1 in Fig. 3(c) reflects the t^{a+} (+ means up or majority spin) state formed by the hybridization of the Cr dε and valence electrons of neighboring Te atoms.

On the other hand, the spectra obtained at a positive bias in the atomic scale are reported for the first time in this study. The peak energies of the dI/dV spectra were different from each other and depended on the position of the measurement. From the comparison of our STS result with those of the theoretical study, we concluded that, in Fig. 3(c), the peaks at $V_s = +1.67$ (in brown and purple curves, indicated by a dotted line) and +1.77 V (in a green curve, indicated by a broken line) can be identified as the energy states derived from the e^- (− means down or minority spin) states originating from Cr dγ states, which very weakly hybridize with the host valence states. Moreover, the large LDOS areas of these states are not located at the row of topmost Te atoms but near that of Cr atoms, as shown by #3 and #4 in Fig. 3(d). This result is also consistent with the conclusion above, because the e states should be located near the substitutional Cr atom owing to the weak hybridization with the host. For a Cr atom in the tetrahedral substitutional site, as in the atomic

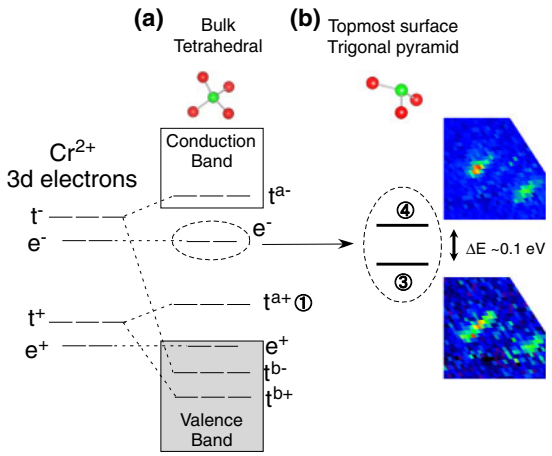

Fig. 4. (Color online) (a) Schematic diagram of energy levels of impurity states induced by Cr^{2+} derived from the results of the previous theoretical study.[17] (b) Schematic explanation for the observed energy splitting of e^- states. As a possible mechanism, energy splitting of e^- states might be induced by the symmetry breaking at the surface.

arrangement of the bulk zinc blende structure, the e^- states are doubly degenerated. The results of our STS measurements indicate that the degeneracy was resolved by symmetry breaking on the surface. For atoms in the topmost (110) surface, the tetrahedral symmetry is broken into the trigonal symmetry owing to the absence of one neighboring atom relative to the bulk configuration. In the trigonal atomic configuration, the two e^- states are not equivalent and split into two distinct states. Although it is difficult to identify the origin of the two states at present, these different spatial distributions should give us essential information for solving the issue. Here, it is also difficult to explain why we could not observe a split of the t state; this is also expected to be resolved by the breaking of the tetrahedral symmetry on the surface. In order to clarify these issues, further study must be carried out from both experimental and theoretical aspects with the precise description of the surface state.

Finally, we mention the peak labeled #5, which appeared at the highest energy in the gap of p-ZnTe. Its LDOS spatial distribution [Fig. 3(d#5)] spreads over 5–6 Å from the position of the doped Cr atoms. From these results, we consider that the state originates from the conduction band of the host ZnTe with some energy shift toward a lower energy. Since the Cr impurity states are formed in the energy gap region of the host p-ZnTe, the acceptor around the Cr atoms is compensated and the level of E_F is shifted toward a deeper energy region in the gap. As a result, the relative position of the energy band of the host p-ZnTe around a Cr atom is shifted toward a lower energy. Since the effect of the compensation spreads over some spatial extent, we observe the states within several angstroms around the Cr atom. The effect of the energy shift appears in the dI/dV–V spectra in the negative sample bias region; the spectra measured around the Cr atom [green, brown, and purple curves in Fig. 3(c)] rise at larger negative V_s values than that over the area without Cr.

4. Conclusions

In this study, we investigated impurity states of Cr atoms in the p-ZnTe(110) surface by STM. We successfully observed single Cr atoms substituting into Zn sites located in the first layer. Our STS measurement revealed the impurity states located around the energy gap region of the host ZnTe. We observed impurity states, which have characteristic energy levels and LDOS spatial distributions, corresponding to the impurity states predicted in an earlier theoretical study.[17] Furthermore, our STS measurement revealed that the degeneracy of the e^- states, which are doubly degenerated in the bulk tetrahedral substitutional site, was clearly resolved by symmetry breaking at the surface.

We believe that the result of this study provides fundamental knowledge for realizing the nanomagnetism based on the DMS of the semiconductor surface in an atomic scale. In the future, with the reduction in the size of electronic devices, such impurity states of a single doped atom will become essential in controlling the performance of the device. Furthermore, we expect that the impurity states will be utilized for the realization and application of single-atom electronics.[22,23]

Acknowledgment

This work was supported by JSPS KAKENHI Grant Numbers 22226003, 24310086, and 25870103.

1) T. Dietl, Nat. Mater. **9**, 965 (2010).
2) T. Dietl and H. Ohno, Rev. Mod. Phys. **86**, 187 (2014).
3) A. M. Yakunin, A. Yu. Silov, P. M. Koenraad, J. H. Wolter, W. Van Roy, J. De Boeck, J.-M. Tang, and M. E. Flatté, Phys. Rev. Lett. **92**, 216806 (2004).
4) A. M. Yakunin, A. Yu. Silov, P. M. Koenraad, J.-M. Tang, M. E. Flatté, W. Van Roy, J. De Boeck, and J. H. Wolter, Phys. Rev. Lett. **95**, 256402 (2005).
5) D. Kitchen, A. Richardella, J. M. Tang, M. E. Flatté, and A. Yazdani, Nature **442**, 436 (2006).
6) A. Stroppa, X. Duan, M. Peressi, D. Furlanetto, and S. Modesti, Phys. Rev. B **75**, 195335 (2007).
7) J. K. Garleff, C. Çelebi, W. Van Roy, J.-M. Tang, M. E. Flatté, and P. M. Koenraad, Phys. Rev. B **78**, 075313 (2008).
8) J. M. Jancu, J. Ch. Girard, M. O. Nestoklon, A. Lemaître, F. Glas, Z. Z. Wang, and P. Voisin, Phys. Rev. Lett. **101**, 196801 (2008).
9) A. Richardella, D. Kitchen, and A. Yazdani, Phys. Rev. B **80**, 045318 (2009).
10) J. K. Garleff, A. P. Wijnheijmer, A. Y. Silov, J. van Bree, W. Van Roy, J. M. Tang, M. E. Flatté, and P. M. Koenraad, Phys. Rev. B **82**, 035303 (2010).
11) D. H. Lee and J. A. Gupta, Science **330**, 1807 (2010).
12) D. H. Lee and J. A. Gupta, Nano Lett. **11**, 2004 (2011).
13) S. Yoshida, M. Yokota, O. Takeuchi, H. Oigawa, Y. Mera, and H. Shigekawa, Appl. Phys. Express **6**, 032401 (2013).
14) J. Bocquel, V. R. Kortan, C. Sahin, R. P. Campion, B. L. Gallagher, M. E. Flatté, and P. M. Koenraad, Phys. Rev. B **87**, 075421 (2013).
15) S. Mühlenberend, M. Gruyters, and R. Berndt, Phys. Rev. B **88**, 115301 (2013).
16) H. Saito, V. Zayets, S. Yamagata, and K. Ando, Phys. Rev. Lett. **90**, 207202 (2003).
17) H. Katayama-Yoshida, K. Sato, T. Fukushima, M. Toyoda, H. Kizaki, V. A. Dinh, and P. H. Dederichs, Phys. Status Solidi A **204**, 15 (2007).
18) S. Kuroda, N. Nishizawa, K. Takita, M. Mitome, Y. Bando, K. Osuch, and T. Dietl, Nat. Mater. **6**, 440 (2007).
19) K. Kanazawa, T. Nishimura, S. Yoshida, H. Shigekawa, and S. Kuroda, Nanoscale **6**, 14667 (2014).
20) A. Wierts, J. M. Ulloa, C. Celebi, P. M. Koenraad, H. Boukari, L. Maingault, R. Andre, and H. Mariette, Appl. Phys. Lett. **91**, 161907 (2007).
21) C. Çelebi, O. Arı, and R. T. Senger, Phys. Rev. B **87**, 085308 (2013).
22) M. Fuechsle, J. A. Miwa, S. Mahapatra, H. Ryu, S. Lee, O. Warschkow, L. C. L. Hollenberg, G. Klimeck, and M. Y. Simmons, Nat. Nanotechnol. **7**, 242 (2012).
23) J. Verduijn, G. C. Tettamanzi, and S. Rogge, Nano Lett. **13**, 1476 (2013).